

Molecular Structure and Morphology of Crosslinked Polyethylene in an Aged Hot-Water Pipe

U. W. GEDDE* and M. IFWARSON

*Studsvik AB, Materials Technology
S-611 82 Nyköping, Sweden*

Internally pressurized crosslinked polyethylene (XLPE) pipes fail according to one of the three following mechanisms: (a) stage I fracture occurs at the highest stresses and is ductile when large defects are absent; (b) stage II fracture is brittle and occurs at intermediate stress levels; (c) stage III fracture occurs at the lowest stress levels and is brittle. It has been assumed that the material in a pipe which fails according to the last mechanism is chemically degraded. This paper presents data obtained by thermal analysis, X-ray diffraction, infrared spectroscopy, and gel permeation chromatography on samples taken at different radial positions from a pipe of XLPE (crosslinked by peroxide) which failed according to the stage III mechanism after 17,136 h when subjected to 2.62 MPa hoop stress at 110°C (internal water/external air). These data are compared with data from samples of an unexposed reference pipe. Highly degraded brown spots, referred to as "oxidation spots", are visible in the aged pipe. The puncture fracture occurred in one of these oxidation spots. The increase in melting point and crystallinity, the decrease in fold surface free energy, the almost invariant crystal unit cell, the decrease in gel content, the decrease in molecular weight of the soluble fraction and the formation of carbonyl and hydroxyl groups at the inner wall in the aged pipe compared with the properties of the unexposed pipe are consistent with an oxidative degradation of the amorphous chain segments including scission of entangled chains and interlamellar tie chains. The latter is the main reason for the major reduction in strength of the aged pipe leading to stage III failure. The thickness of the inner wall layer of highly oxidized material was about 5 mm in the oxidation spots and only 0.5 mm elsewhere in the aged 10 mm thick pipe.

INTRODUCTION

The use of crosslinked polyethylene (XLPE) has experienced a growth in a variety of applications, e.g. in insulations in medium and high voltage cables and in pipes for domestic low-temperature heat-distribution systems. The demand for high reliability in the pipe systems requires extensive testing. Internal pressurizing tests must be performed at a great number of stress levels at different temperatures and the engineering stress corresponding to a 50 year life is determined by extrapolation. *Fig. 1a* shows the three stages of fracture which have been observed in XLPE pipes (1). (a) Stage I fracture is ductile when large defects are absent and it has been established that chemical effects in the polymer are insignificant (2). (b) Stage II fracture is brittle and the chemical degradation of the material is limited (2). (c) Stage III fracture is brittle and the material is chemically degraded, which is also demonstrated by the weak

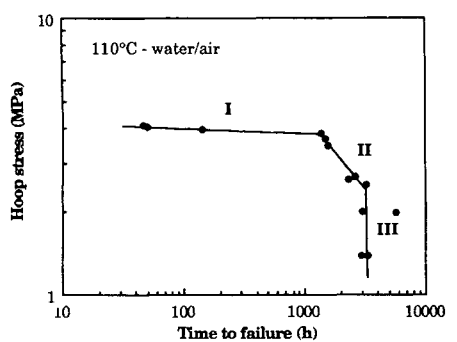
stress dependence of the failure time of the stage III curve (2). XLPE pipes with a normal degree of crosslinking (>70% gel content) display only stage I and stage III failure (*Fig. 1b*). One important implication of the almost vertical stage III failure line (*Fig. 1*) is that the criterion for a 50-year life may often be based only on temperature rather than on both stress and temperature.

This paper presents data obtained by thermal analysis (DSC and DTA), X-ray diffraction (WAXS), infrared (IR) spectroscopy and gel permeation chromatography (GPC) on samples taken at different radial positions in the wall of a pipe which had failed according to stage III fracture. Reference data for samples taken from an unexposed pipe are also presented. A qualitative description of the degradation of the pipe material is finally presented.

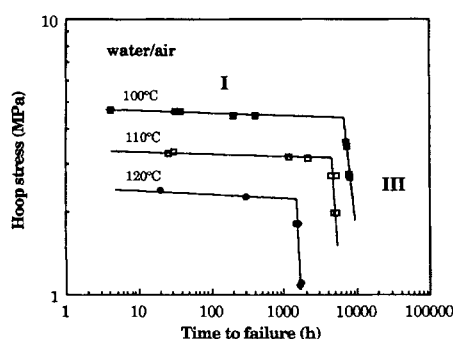
EXPERIMENTAL

A 110 ± 0.5 mm pipe (experimental quality) of XLPE was produced by the Engel method by Wirsbo Bruks AB, Sweden. Data for polymer prior to crosslinking: grade: Lupolen 5261-Z[®], $M_w = 303\,000$,

* Address: Department of Polymer Technology, The Royal Institute of Technology, S-100 44 Stockholm, Sweden.



(a)



(b)

Fig. 1. Typical long-term fracture data for XLPE with (a) a low crosslinking density displaying all three stages of failure (I-III); (b) a normal crosslinking density displaying only stage I and stage III failure.

$M_n = 20,000$; linear PE; stabilized with 0.25% (w/w) Irganox 1035[®] (2,2'-thiodiethylbis-[3-(3,5-di-tert.butyl-4-hydroxyphenyl)-propionate]), 0.07% (w/w) Irganox 1076[®] (octadecyl 3-(3,5-di-tert.butyl-4-hydroxyphenyl)-propionate) and 0.25% (w/w) UV absorber CYASORB UV 531[®] (2-hydroxy-4-n-octoxy-benzophenone). The content of the crosslinking peroxide, di-tert.butylperoxide added to this polymer was 0.4% (w/w). The thickness of the pipe wall was 10 mm. Two pipes were compared in this study: (a) *Unexposed pipe*; (b) a pipe, referred to as *aged pipe*, fractured in an internal pressurizing test according to stage III failure after being subjected to a constant hoop stress of 2.62 MPa at $110 \pm 2^\circ\text{C}$ for 17,136 h. The pipe was subjected internally to water and externally to air. Details of the internal pressurizing test have been published earlier (1). The brass fittings used in the experiments have some catalytic effect on the thermal oxidation of the XLPE grade used in the studies (3). Fracture did not, however, occur near the fittings (3). Several brown spots containing numerous microcracks were found in the inner wall surface of the pipe. The puncture failure was found in one of these "oxidation spots." Figure 2 provides a picture of the distribution of the oxidation spots in the wall of the aged pipe.



Fig. 2. Photograph of the aged pipe showing oxidation spot (indicated by arrow). Note the cracks present in the oxidation spot.

DSC was carried out in a temperature- and energy-calibrated Perkin-Elmer DSC-7 equipped with a Perkin-Elmer 7700 computer. Disk-shaped samples, weighing 5–10 mg and having a thickness of 0.2–0.5 mm and a diameter of 5 mm originally cut from cylinders which had been radially punched through the pipe wall, were heated at a rate of $10^\circ\text{C}/\text{min}$ and melting thermograms were recorded. Samples were taken both from the oxidation spots and elsewhere from the inner wall region of the aged pipe. The melting peak temperature (T_m) and mass crystallinity (w_c) were determined, the latter being determined according to the equation:

$$w_c = \Delta h / \Delta h^\circ \quad (1)$$

where Δh is the heat of fusion for the sample and Δh° is the heat of fusion for 100% crystalline material and is for PE equal to 293 kJ/kg (4). DTA was carried out in a Mettler TA-3000 system equipped with a DSC 20 Standard Cell and a TC10A TA Processor. The thermal stability was measured at a $10^\circ\text{C}/\text{min}$ heating rate from 20°C to 250°C using oxygen as purge gas (flow rate: 50 ml/min), the temperature corresponding to the onset of the exothermic oxidation reaction, the so-called oxidation temperature, T_{ox} , being recorded. The latter is defined by the intersection of the extrapolated scanning base line and the tangent at a point on the curve which deviates 0.5 mW from the scanning base line. A number of samples, linear PE sharp fractions: $M_w = 2,500, 14,000, 32,000,$ and $193,000$ ($M_w/M_n \approx 1.1-1.2$) and a branched fraction: $M_w \approx 100,000, M_w/M_n \approx 5.1.4$ mole % of ethyl branches, containing no antioxidant were tested to determine T_{ox} for completely unstabilized polymer.

Wide-angle X-ray scattering (WAXS) was performed on two 150 μm samples: (a) Unexposed pipe, $x = 5$ mm; (b) Aged pipe, oxidation spot, $x = 0.1$ mm. The analysis was performed in a focusing Guinier-Hägg camera with transmission geometry. Strictly monochromatized $\text{CuK}\alpha_1$ radiation with $\lambda = 0.154060$ nm and single coated films were used. The accuracy of the measured Bragg angles was tested by photographs taken with silicon added as internal theta standard. The use of an internal standard reduces zero-point errors to a negligible level, corrects for film shrinkage and makes it possible to correct for geometrical errors in the camera. The films were evaluated by a computer-controlled single-beam microdensitometer.

Samples (5 mm diameter) cut from the pipe wall at different distances from the inner wall were studied by Frustrated Multiple Internal Reflectance Infrared (FMIR-IR) spectroscopy (Perkin-Elmer 1710 Fourier Transform Infrared Spectrometer). Each spectrum is based on 50-500 scans. The spectra for a number of well-defined substances, 1-octene, 1-octadecene, 5-nonanone, dodecanedioic acid and a polyester based on butanediol and decanedioic acid were determined to calibrate the different carbonyl, hydroxyl and vinyl absorption bands.

The soluble fractions (denoted SOL) of five different samples taken from the different pipes at the following locations (x is the distance from the inner wall surface): (a) aged pipe, oxidation spot, $x = 0-2$ mm; (b) aged pipe, oxidation spot, $x = 4-6$ mm; (c) aged pipe, oxidation spot, $x = 8-10$ mm; (d) unexposed pipe, $x = 0-2$ mm; (e) unexposed pipe, $x = 4-6$ mm were analyzed by GPC. Pieces, about 0.2 mm thick, from the samples were treated under agitation with *p*-xylene at 130°C for 24 h. The concentration of dissolved polymer was always less than 1 wt %. To the solution, which was separated from the swollen XLPE residues, an excess of methanol was added to precipitate the dissolved polymer. The system was kept at 0°C for about 15 h to ensure complete precipitation. After centrifugation, the PE crystals were separated from the solution by decanting, and the precipitate was dried *in vacuo* to constant weight.

The gel permeation chromatography (GPC) carried out by Dr. S. Holding at RAPRA Technology Ltd, Great Britain involved the dissolution of 20 mg samples in 1,2-dichlorobenzene stabilized by 2,6-di-*t*-butyl *p*-cresol at 150°C. After filtration, the sample solutions were injected into the P.L. gel column which was thermostat-controlled at 130°C and equipped with an IR detector recording at 3.4 μm . The data were analyzed using the "universal" calibration procedure with the Mark-Houwink parameters for HDPE.

RESULTS AND DISCUSSION

The crystallinity (w_c) data presented in Fig. 3 show that w_c is lower at both the inner and the outer surfaces than in the middle of the wall of the unexposed pipe. This relatively small (3%) variation in w_c

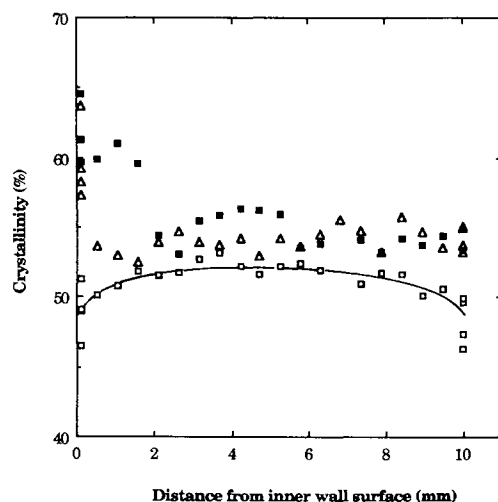


Fig. 3. Mass crystallinity (in %) plotted versus the distance from the inner wall surface: □ unexposed pipe; ■ aged pipe, oxidation spot; △ aged pipe, outside oxidation spots.

is due to the cooling rate gradient prevailing during crystallization in the post-extrusion phase. Samples taken from the aged pipe exhibit a higher crystallinity than those taken from the unexposed pipe. In the aged pipe w_c is also strongly dependent on the radial position in the pipe wall (Fig. 3). The maximum crystallinity (62%) was found in samples taken at the inner surface in the oxidation spots. For the samples taken from the oxidation spots these high w_c values occur at distances from the inner surface between $x = 0$ and 2 mm. Crystallinity is almost constant, between 54 and 55%, for samples taken at a depth of $x \geq 2$ mm. For the samples taken from regions outside the oxidation spots of the aged pipe the maximum w_c value at the inner wall is about 60% and the constant value of about 54% is established considerably closer to the inner wall, i.e. at $x = 0.5$ mm.

Table 1 presents a comparison between the crystallinity data obtained by DSC presented in this paper and data obtained by density measurements presented in a previous paper (7). The agreement between the two sets of data is good.

Figure 4 presents a comparison of the melting peak temperature (T_m) for samples taken from unexposed pipe and from aged pipe. The T_m value is 1°C higher for samples taken from the middle of the wall of the aged pipe. The melting points of the samples taken from the inner wall surface (oxidation spots) are 5-6°C higher in the aged pipe than in the unexposed pipe. The melting point decreases with depth x until finally an approximately constant value is reached at $x = 2$ mm. The increase in melting point of the inner wall samples taken from other areas in the aged pipe is less dramatic, only 3°C and the thickness of the layer with a melting point gradient is about 0.5 mm.

The melting point data indicate that the crystal thickness has increased due to the prolonged treatment of the polymer at 110°C. The melting point data

Table 1. Summary of DSC Data.

Pipe	x^a (mm)	w_c (%)	$\Delta v_c/v_{cu}^b$	$\Delta v_c/v_{cu}^c$	T_m^{od} (°C)	L_c^e (nm)	$\Delta L_c/L_{cu}^f$	σ'/σ^g
Unexp.	0	49.0	—	—	127.5	18.6	—	1
Unexp.	5	52.3	—	—	128.6	20.2	—	1
Unexp.	10	48.5	—	—	125.7	16.5	—	1
Aged ^h	0	62.0	0.32	—	132.3	28.0	0.51	0.88
Aged ⁱ	0	60.0	0.27	0.21	130.5	23.6	0.27	1
Aged	5	54.5	0.06	0.04	129.7	22.0	0.09	0.97
Aged	10	54.0	0.15	0.09	129.1	20.9	0.27	0.93

^a Distance from inner wall surface.

^b Relative increase in volume crystallinity according to DSC relating to the crystallinity of sample of unexposed pipe (v_{cu}): $\Delta v_c/v_{cu} = [v_c(x) - v_{cu}(x)]/v_{cu}(x)$. The volume crystallinity have been calculated as follows: $v_c = 1/[1 - (\rho_c/\rho_a)(1 - w_c)/w_c]$ (2)

The increase in amorphous density by oxidation is estimated by combining the data presented in Table 2 with density data on aliphatic polyesters collected by Wunderlich (5).

^c Relative increase in volume crystallinity obtained by density measurements⁷ relating to the crystallinity of sample of unexposed pipe (v_{cu}): $\Delta v_c/v_{cu} = [v_c(x) - v_{cu}(x)]/v_{cu}(x)$.

^d Melting peak temperature corrected for parallel crystal growth and superheating according to Ref. 6.

^e Crystal thickness calculated according to Eq 3 from melting point data. The material parameters (T_m^o , etc) are shown in the text.

^f Relative increase in crystal thickness with respect to crystal thickness of sample of unexposed pipe (L_{cu}): $\Delta L_c/L_{cu} = [L_c(x) - L_{cu}(x)]/L_{cu}(x)$.

^g σ and σ' are the fold surface free energies of the crystals in unexposed and aged pipes, respectively.

^h Samples taken from "oxidation spots".

ⁱ Samples taken from other areas.

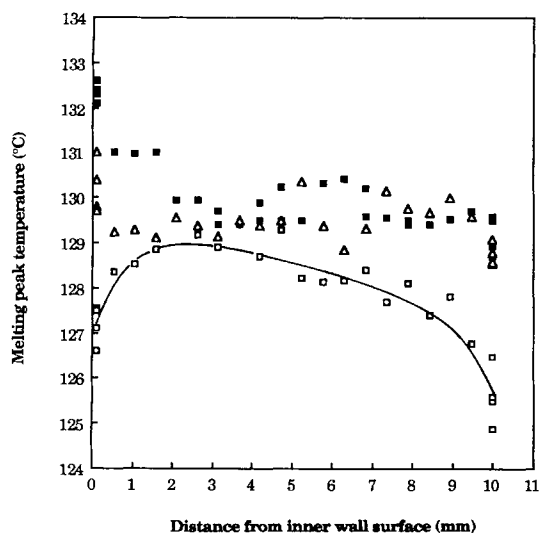


Fig. 4. Melting peak temperature plotted versus the distance from the inner wall surface: □ unexposed pipe; ■ aged pipe, oxidation spot; △ aged pipe, outside oxidation spots. The presented data are corrected for thermal lag and parallel crystal growth and super-heating according to Ref. 6.

can be transformed into crystal thickness data using the Thomson-Gibbs equation (Eq 3):

$$T_m = T_m^o [1 - 2\sigma/(\Delta h^o \rho L_c)] \quad (3)$$

where T_m^o is the equilibrium melting point, 415 K (4), σ is the fold surface free energy, 93 mJ/m² (4), Δh^o is the heat of fusion, 293 kJ/kg (4), ρ is the crystalline phase density, 1000 kg/m³ (5), and L_c is the crystal thickness. The results of these calculations are presented in Table 1. The relative increase in apparent crystal thickness ($\Delta L_c/L_{cu}$) of the material in the central region of the pipe wall amounts to 9%. A significantly larger increase in apparent crystal thickness is revealed for the inner wall material, 51% in oxidation spots and 27% in other areas, and for the outer wall material, 27%. It should be noted, however, that the accuracy of these data is limited since even a small change in recorded melting point has a sig-

nificant effect on the relative increase in crystal thickness. In addition, parallel crystal growth and superheating of the samples, although corrected for in the analysis, further reduce the accuracy of the thickness data.

Table 1 shows that the $\Delta L_c/L_{cu}$ values are higher than the corresponding values of the relative increase in volume crystallinity ($\Delta V_c/V_{cu}$) obtained by DSC and density measurements. The latter values are based on two established and accurate experimental techniques. The crystal thickness determination is however indirect and relies on the invariance of T_m^o , Δh , ρ and σ in Eq 3. The question is whether these parameters are affected by aging. The first three parameters depend on the bulk properties of the crystals and should be invariant if degradation is confined to the amorphous component. However, X-ray diffraction reveals some expansion in the a dimension of the orthorhombic unit cell in the aged sample: $a = 0.7433$ nm, $b = 0.4949$ nm, $c = 0.2552$ nm, volume = 0.09388 (nm)³ (unexposed sample); $a = 0.7460$ nm, $b = 0.4955$ nm, $c = 0.2563$ nm, volume = 0.09474 (nm)³ (aged sample). The effect on T_m^o , Δh and ρ is small and cannot explain the major difference between data for $\Delta L_c/L_{cu}$ and $\Delta V_c/V_{cu}$ in the highly degraded aged sample.

The fold surface free energy σ is however sensitive to the nature of fold surface which in turn is likely to be affected by possible degradation. Table 1 presents data for the required reduction in σ , i.e. σ'/σ (σ' and σ are the fold surface free energies of the crystals in the aged and unexposed pipe respectively) which brings the $\Delta L_c/L_{cu}$ data into agreement with the $\Delta V_c/V_{cu}$ data. The inner wall samples taken from oxidation spots of the aged pipe display the strongest decrease in fold surface free energy, close to 12% (Table 1). The corresponding reduction for samples from the middle of the aged pipe wall is less than 3% and for the outer surface material it amounts to about 7%.

The oxidation temperature (T_{ox}) is greatest in the middle of the pipe wall and falls about 10–20°C at both the inner and outer surfaces of the unexposed

pipe (Fig. 5). In the aged pipe, T_{ox} drops drastically at the inner surface. There seems to be a minimum value for T_{ox} of about 165°C. The thickness of the layer with such a low value of T_{ox} varies significantly: from 4–5 mm in samples taken from the oxidation spots to 0.5 mm in samples taken elsewhere. A smaller but still significant decrease in T_{ox} is also indicated for the outer wall material of the aged pipe.

A number of LPE and BPE fractions containing no antioxidants were tested and gave T_{ox} values between 175 and 185°C. After the initial heating to 200°C, one of these samples was cooled to 20°C displayed, and on reheating it gave a T_{ox} value of 147°C. This clearly shows that T_{ox} is related not only to the content of remaining antioxidant but also to the molecular structure of the polymer.

IR spectroscopy demonstrates that the aged pipe has been thermally oxidized (Fig. 6). A number of strong absorption bands have developed in the samples of the aged pipe: (a) 3 200–3 700 cm^{-1} (composite band assigned to both hydroperoxide and hydroxyl groups), (b) 1790 cm^{-1} (carbonyl, peracid), (c) 1763 cm^{-1} (carbonyl, perester), (d) 1740 cm^{-1} (carbonyl, ester), (e) 1715 cm^{-1} (carbonyl, ketone), (f) 1705 cm^{-1} (carbonyl, acid), (h) 1170 cm^{-1} (ether bridges). The 1465 cm^{-1} band (g) assigned to methylene groups is used as internal standard. The different absorption bands have been assigned according to Loungo (8) and Grafmüller and Husemann (9). A number of strong absorption bands occurring between 1680 cm^{-1} and 1500 cm^{-1} were observed in the samples taken from the aged pipe (Fig. 1). The absence of absorption bands at 985–1005 cm^{-1} and 900–920 cm^{-1} (vinyl), 880–900 cm^{-1} (vinylidene), 960–990 cm^{-1} (transvinylene), 675–725 cm^{-1} (cis-vinylene) and bands occurring between 795 cm^{-1} and 980 cm^{-1} associated with these groups and ketonic and ester carbonyl groups shows that the absorption bands between 1600 and 1680 cm^{-1} cannot be related to unsaturation. It should be noted that the molar coefficient of extinction for the bands near 1000 cm^{-1} is

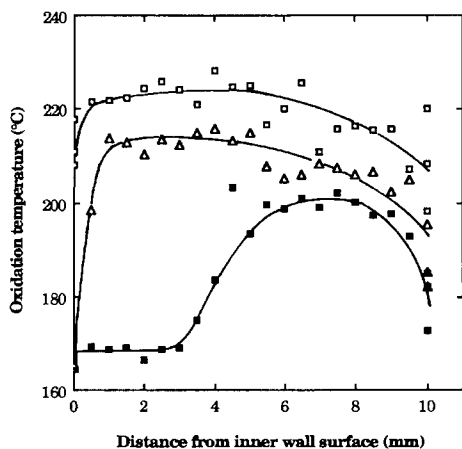


Fig. 5. Oxidation temperature plotted versus the distance from the inner wall surface: \square unexposed pipe; \blacksquare aged pipe, oxidation spot; \triangle aged pipe, outside oxidation spots.

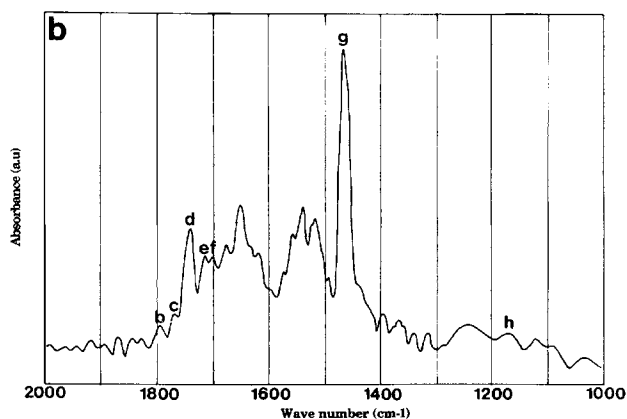
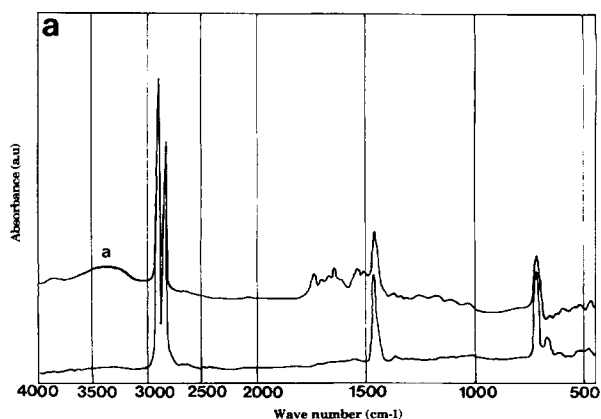


Fig. 6. Infrared (IR) absorbance spectra (a) lower spectrum: unexposed pipe, $x = 0$ mm; upper spectrum: aged pipe, $x = 5$ mm; (b) aged pipe, $x = 5$ mm. Absorption bands which are further discussed in this paper are denoted a to h. The assignment of these bands is found in the text.

about the same as that for the 1650 cm^{-1} band. It is known that water, free or bound, has absorption bands near 1600 cm^{-1} and it is suggested that the absorption bands between 1680 cm^{-1} and 1500 cm^{-1} are due to the presence of small traces of water in the oxidized samples.

Figure 7 presents data for the relative absorbance of absorption bands assigned to ester carbonyl and hydroxyl groups plotted as a function of the radial distance (x) from the inner wall surface. It should be noted that the differences in penetration depth (d_p) for bands of different wave lengths (λ) are taken into consideration. It is assumed that d_p is equal to $\lambda/10$ (10). Samples taken from the oxidation spots possess high absorbance values for these bands at $x < 5$ mm. More peripheral samples ($x \geq 7$ mm) exhibit approximately constant and relative low absorbance values, although the relative absorbance values for these samples are still higher than those obtained for the unexposed pipe ($A_{1740} \approx 0.05$ – 0.06). Samples taken outside the oxidation spots in the aged pipe exhibit high absorbance values of the three bands at the inner wall surface but the highly oxidized inner wall skin is only 0.5 mm. A few cross-sections displayed somewhat higher absorbance values ($A_{1740} \approx 0.4$) in the middle ($x \approx 5$ mm) than shown in Fig. 7b. The

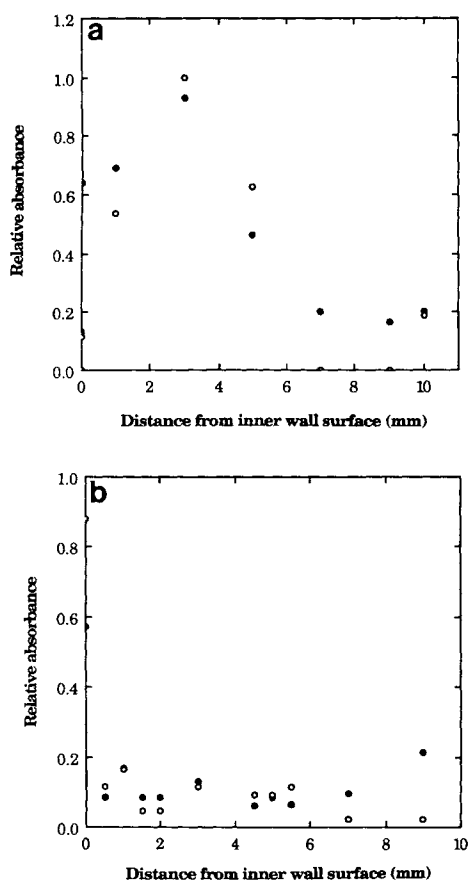


Fig. 7. Relative absorbance (normalized with respect to the 1465 cm^{-1} band) of two different absorption bands: 3400 cm^{-1} (O) and 1740 cm^{-1} (●) for samples of aged pipe: (a) oxidation spots; (b) outside oxidation spots.

middles of these cross-sections were always yellow indicating significant thermal oxidation of this material.

Figures 8 and 9 show that the relative absorbance values (each normalized with respect to the 1465 cm^{-1} band) of the different absorption bands is linearly interrelated, i.e. the relative proportion of the different groups assigned to these absorption bands is about the same independent of the "degree" of oxidation. The scatter in the data, typically amounting to 0.1 in relative absorbance, may be explained by the overlap of adjacent absorption bands.

The experimental absorption spectra of three of the samples were analyzed in order to resolve the different single absorption peaks. The relative absorption values obtained directly from the experimental spectra for bands with strong neighbouring bands closer than 15 cm^{-1} are about 20% greater than the values obtained from the resolved peaks.

Absorption bands associated with ketonic carbonyls (1715 cm^{-1}), ester carbonyls (1740 cm^{-1}) and acidic carbonyls (1705 cm^{-1}) were calibrated by running a number of spectra of compounds of known composition. The constant K in the equation:

$$x \text{ (mole\%)} = KA_x/A_{1465} \quad (4)$$

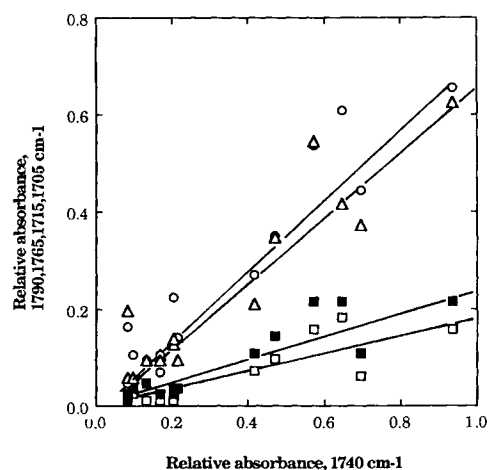


Fig. 8. Relative absorbance at 1790 cm^{-1} (□), 1765 cm^{-1} (■), 1715 cm^{-1} (O), 1705 cm^{-1} (Δ) plotted versus relative absorbance at 1740 cm^{-1} . The absorbance values are normalized with respect to the 1465 cm^{-1} methylene band.

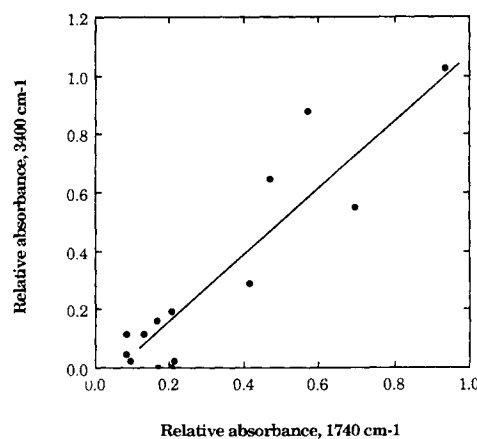


Fig. 9. Relative absorbance at 3400 cm^{-1} plotted versus relative absorbance at 1740 cm^{-1} . The absorbance values are normalized with respect to the 1465 cm^{-1} methylene band.

was determined and the following values were obtained: 1740 cm^{-1} : $K = 2.7$; 1705 cm^{-1} : $K = 3.6$; 1715 cm^{-1} : $K = 7-14$. The uncertainty in the K value of the 1715 cm^{-1} band is due to the presence of nearby overlapping peaks in the spectra of the calibration substances. Table 2 presents a summary of the molecular structure data obtained by IR.

The concentrations of ester and acid groups are both about 1-2% in the highly oxidized zone (Table 2). The concentration of ketones is about 2-3 times greater, 2.5-3.6%, than the concentration of ester and acid groups.

Molecular weight data for the soluble (SOL) fractions obtained by GPC are presented in Table 3. The samples taken from the aged pipe have significantly lower M_w and M_n values than those from the unexposed pipe. The inner wall material of the aged pipe exhibits the most pronounced decrease in molecular weight. The relative reduction in M_w for samples of the aged pipe with respect to those from the unex-

Table 2. Concentration (mole%) of Different Carbonyl Groups.

Group	$x = 0^a$	$x = 1^b$	$x = 3^b$	$x = 9^b$
Ester	1.2	1.5	2.0	0.4
Carboxylic acid	1.6	1.0	2.0	0.25
Ketone	3.0	2.5	3.6	0.5

^a From aged pipe, outside oxidations spots, x in mm.^b From aged pipe, oxidation spots, x in mm.**Table 3. Molecular Weight Data for SOL Fractions.**

Sample	$M_w \times 10^{-3}$	$M_n \times 10^{-3}$	M_w/M_n
Unexposed $x = 0-2$ mm	73	13.4	5.6
Unexposed $x = 4-6$ mm	115	12.5	9.2
Aged $x = 0-2$ mm	30.5	6.4	4.8
Aged $x = 4-6$ mm	51.5	9.3	5.5
Aged $x = 8-10$ mm	49.9	9.8	5.1

posed pipe lies between 1.9 and 3.1. The corresponding reduction in M_n is 1.3 to 2.0. Further evidence for the dominance of chain scission in the thermal oxidative degradation of this particular pipe was presented in a previous paper (7). It was shown that the gel content in the aged pipe decreased by 1–2% in the middle part of the pipe wall and by 8% at the inner surface.

Figures 10 and 11 show that both melting peak temperature and crystallinity are almost independent of A_{1740} for A_{1740} values lower than 0.4. Above the latter value there is a strong increase in both these quantities with increasing A_{1740} .

Figure 12 shows that the oxidation temperature falls from 220°C to 180°C when A_{1740} increases from 0.1 to 0.2. Unoxidized samples of PE containing no antioxidant display T_{ox} values between 175 and 185°C. A slow oxidation process, indicated by the small increase in A_{1740} , thus occurs parallel with the consumption of the antioxidant. In the T_{ox} range below 180°C, A_{1740} increases strongly with decreasing T_{ox} , due to the fact that these samples contain essentially no effective antioxidant at this stage and oxidation progresses rapidly.

For T_{ox} values greater than 170°C there is only a minor change in melting point and crystallinity with increasing oxidation temperature (Figs. 12 and 13). This again corresponds to the phase when the antioxidant is consumed and partially protects the polymer from degradation. Below 170°C in T_{ox} there is a dramatic increase in both melting peak temperature and crystallinity with decreasing T_{ox} , which reflects the significant oxidative degradation in these samples.

The scattering in the data presented in Figs. 10–14 is due primarily to the fact that these cross-correlations are obtained from analyses of different samples taken at the same distance from the inner wall surface.

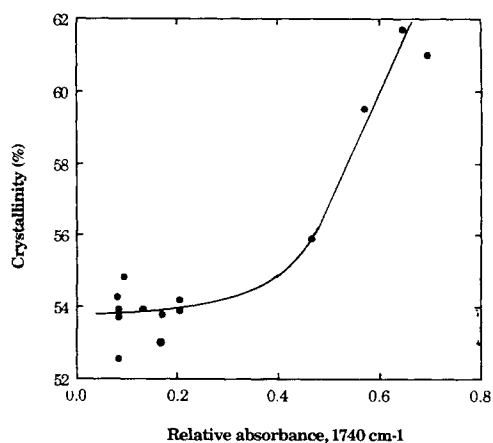


Fig. 10. Mass crystallinity (in %) for samples taken from the aged pipe plotted versus relative absorbance at 1740 cm^{-1} (by IR; normalized with respect to the 1465 cm^{-1} methylene band).

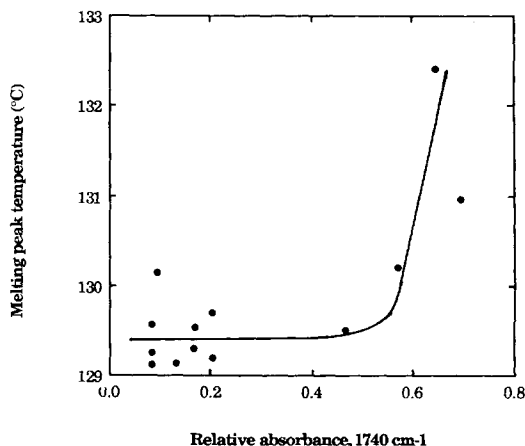


Fig. 11. Melting peak temperature for samples taken from the aged pipe plotted versus relative absorbance at 1740 cm^{-1} (by IR; normalized with respect to the 1465 cm^{-1} methylene band).

The aging of the XLPE pipe, with pressurized water on the inside and air of normal pressure on the outside, occurs by thermal oxidation. IR spectroscopy shows the existence of a number of different carbonyls and hydroxyl groups in the aged polymer. The total content of carbonyls in the highly oxidized material is about 5 mole%.

Chain scission, revealed by both GPC and gel content data, is perhaps the most important effect of the thermal oxidation. The localization of the degradation process to the amorphous component is here confirmed by X-ray diffraction. The expansion of the unit cell a dimension from 0.743 nm in an unexposed sample to 0.746 nm in an oxidized sample with 5 mole% of carbonyl groups is only 30% of the change recorded for a sample with homogeneously distributed carbonyls (4). The expansion of the unit cell can be explained by the inclusion of carbonyls in crystalline material which has been molten during aging at 110°C. Numerous reports in the literature, e.g. Refs. 11–13, support this view. Thus, the amorphous

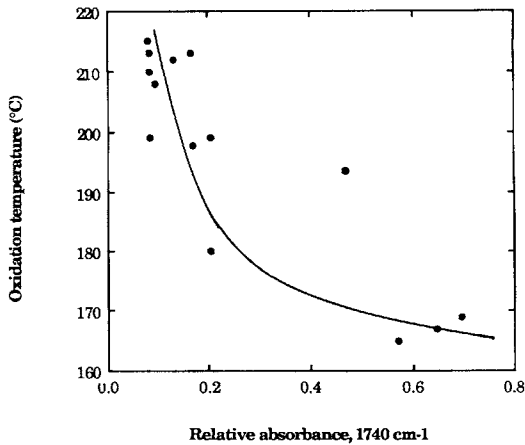


Fig. 12. Oxidation temperature for samples taken from the aged pipe plotted versus relative absorbance at 1740 cm^{-1} (by IR; normalized with respect to the 1465 cm^{-1} methylene band).

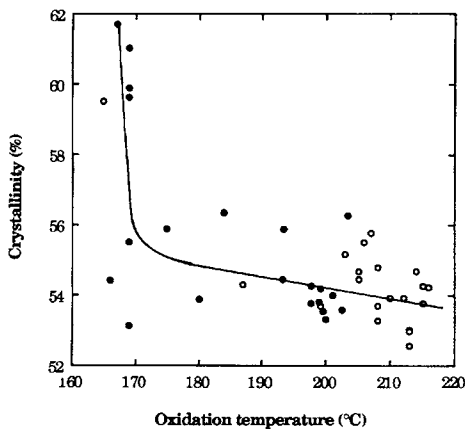


Fig. 13. Mass crystallinity (in %) for samples taken from the aged pipe (● oxidation spots; ○ outside oxidation spots) plotted versus oxidation temperature.

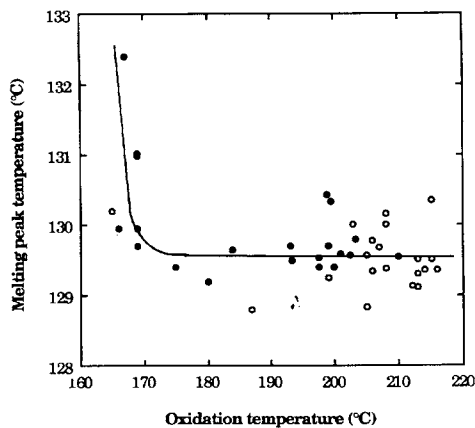


Fig. 14. Melting peak temperature for samples taken from the aged pipe (● oxidation spots; ○ outside oxidation spots) plotted versus oxidation temperature.

chain segments, loops, tie chains and cilia, are chemically changed by the introduction of the aforementioned groups and by less frequently occurring chain scissions. The latter must be responsible for the ex-

treme brittleness of the material in the oxidation spots of the aged pipe.

Thermal analysis reveals an increase in mass crystallinity and melting point of the highly oxidized material. This has been earlier reported by several authors (12, 13) and may be explained on the basis of disentanglement of segments in which chain scission has occurred followed by crystal growth along the chain axis. The reduction in fold surface free energy amounting to 12% in the highly oxidized samples is an interesting and not hitherto reported observation. It is, however, known from crystallization kinetics and melting point data on linear PE sharp fraction that the fold surface free energy increases strongly with molecular weight, approaching a constant value of 93 mJ/m^2 for material of infinitely high molecular weight (14). This can in molecular terms be understood by the increase of chain folding in crystals of higher molecular weight. The work associated with folding the chain is appreciable, about 6 times greater than the energy associated with the crystal-amorphous phase contact. The 12% reduction in fold surface free energy may be due to the "perfection" of the fold surface primarily by elimination of some chain folds. The latter is enhanced by chain scission.

The cause of the oxidation spots can only be speculated on. The most likely reason is that the antioxidant was heterogeneously distributed in the pipe. A very important question which has to be addressed is why the oxidation is confined to the inner wall region. Obviously, the oxygen necessary for oxidation comes from the outside and the surrounding air. If the oxygen consumption, i.e. the oxidation process, is slow compared with the transport of oxygen through the pipe wall, an equilibrium concentration of oxygen should be established through the pipe wall. There will be a greater tendency for antioxidant to be lost at the inner wall surface since transport into the internal water occurs more readily than into the external air phase. Thus, the external air is the source for the oxygen but degradation is concentrated to the inner wall due to the more readily occurring migration of antioxidant. Another possibly important factor is the presence of catalytic Cu ions in the internal water. A model of the degradation process considering these factors will be presented in a coming paper.

It is practical and simple to assess the oxidative stability of a sample by measuring an induction time under isothermal conditions or an oxidation temperature during a temperature scan. The T_{ox} value obtained for a sample is related not only to the remaining content of antioxidant but also to the molecular structure of the polymer. It is also evident that a slow oxidative degradation has occurred in the middle regions of the aged pipe wall despite the fact that a significant amount of antioxidant remains in the sample. Thus, it seems that the antioxidant is less effective at temperatures below the melting point of the polymer and more effective at temperatures above the melting point of the polymer. This may be due to segregation of the antioxidant at the lower

temperatures in the semicrystalline state and better mixing at higher temperatures when the polymer is molten.

ACKNOWLEDGMENTS

The reported studies are parts of a research program on the long-term properties of polyolefine pipes sponsored by the basic research fund at Studsvik AB, Sweden. The X-ray diffraction work by Dr. Allan Brown, Studsvik AB and the experimental assistance of Mr. Pontus Alm, Department of Polymer Technology, RIT are gratefully acknowledged.

REFERENCES

1. M. Ifwarson and P. Eriksson, *Kunststoffe*, **76**, 245 (1986).
2. P. Eriksson and M. Ifwarson, conf. paper: "Plastic Pipes VI," Plastic and Rubber Institute, York, U.K., 1985.
3. M. Ifwarson, Studsvik AB, Sweden, unpublished data.
4. B. Wunderlich, *Macromolecular Physics, Volume 3: Crystal Melting*, Academic Press, New York (1980).
5. B. Wunderlich, *Macromolecular Physics, Volume 1: Crystal Structure, Morphology, Defects*, Academic Press, New York (1973).
6. U. W. Gedde and J-F Jansson, *Polymer*, **24**, 1521 (1983).
7. E. Figueroa, *Thermochimica Acta*, **114**, 115 (1987).
8. J. P. Luongo, *J. Polym. Sci.*, **42**, 139 (1960).
9. F. Grafmüller and E. Husemann, *Macromol. Chem.*, **40**, 161 and 170 (1960).
10. W. Klöpffer, *Introduction to Polymer Spectroscopy*, Springer Verlag, Berlin, Heidelberg, New York and Tokyo (1984).
11. W. L. Hawkins, W. Matryek, and F. H. Winslow, *J. Polym. Sci.*, **41**, 1 (1959).
12. F. H. Winslow, C. J. Aloisio, W. L. Hawkins, W. Matryek, and S. Matsuoka, *Chem. Ind. (London)*, **533**, (1963).
13. F. H. Winslow, C. J. Aloisio, W. L. Hawkins, W. Matryek, and S. Matsuoka, *Chem. Ind. (London)*, **1465** (1963).
14. J. D. Hoffman, L. J. Frolen, G. S. Ross, and J. I. Lauritzen Jr., *J. Res. Natl. Bur. Stand. (A)*, **6**, 671 (1975).